THE OPTIMUM PERIOD OF THE ELECTRODE STRUCTURE ON A SHUTTLE HARVESTER

Svein Husa[1]*, Cuong Phu Le[2]
[1]Dept of Technology, [2]Dept of Micro and Nano Systems Technology, Vestfold University College, Horten, Norway
*Presenting Author: Svein.Husa@hive.no

Abstract: We model an electrostatic energy harvester of the shuttle type. The electrode capacitances are analytically determined and the model accurately accounts for the power generation when the vibration of the mass is known. We use the model to determine the optimum period of the electrode structures on the mass and the frame, with respect to the generated power. With a given gap between mass and frame, we find the best balance between generated voltage and low output reactance when the period equals 30 times the gap. We also see that we approach a linear relation between vibration amplitude and power output when the amplitude is much larger than the period of the electrode pattern.

Keywords: Shuttle harvester, optimal electrode periodicity, fringing capacitance.

INTRODUCTION

Electrostatic harvesters making use of the capacitance changes that are set up by variation in the overlap between one or more pairs of finger electrodes fixed to the vibrating mass and the frame, by in-plane motion, are often referred to as shuttle harvesters. Shuttle harvesters have been successfully designed and fabricated by many research groups. They possess a property not found in other harvester structures; with a proper choice of the period of the electrode pattern and the vibration of the seismic mass, the frequency content of the generated voltage can be many times higher than the frequency of the mass motion. This is demonstrated in devices designed and fabricated in the past [1], [2].

Since the internal impedance of the electrostatic generator is mainly capacitive, the matched load will go down and the output power will increase, when the frequency increases. Reducing the period of the electrode structure in order to generate harmonic voltage components, also has a negative effect. It makes the variation range of the inter-electrode capacitances decrease, and this in turn reduces the generated voltage. It is clear that an optimum must exist between the extremes. This feature has not been much studied in the past. We have reported an analytic approach [3]. Recently a numeric simulation and analysis covering several design parameters, among them the periodicity of the finger electrodes, was published [4]. Our present work has a more restricted scope since it mainly focuses on the interplay between gap size, finger electrode period and the vibration amplitude.

MODELLING APPROACH

Device structure

The basic structure of our harvester is shown in Fig. 1. The vibrating mass is conducting silicon. It is electrically grounded to the static device frame through the silicon springs. The surface facing the gap is insulated by an oxide layer of thickness *d*, and a periodic pattern of biased electrode stripes is defined on the oxide surface. In practical devices we try to use an electret material [5], but for our modeling we might as well consider them as biased metal stripes. The other set of electrodes are conducting stripes on a glass surface.

The working electrodes are connected in parallel to the load, R. The electrode sets have the same periodicity, *p*, and the width between the stripes is *p/2*. The gap between the mass and the frame is *g*. The transverse width of the electrode structure is *w*. While *w, p* and *g* are important model parameters, the effect of the dielectric layer, *d*, is small as long as it is much smaller than *g*, which is true in all cases we have seen until now.

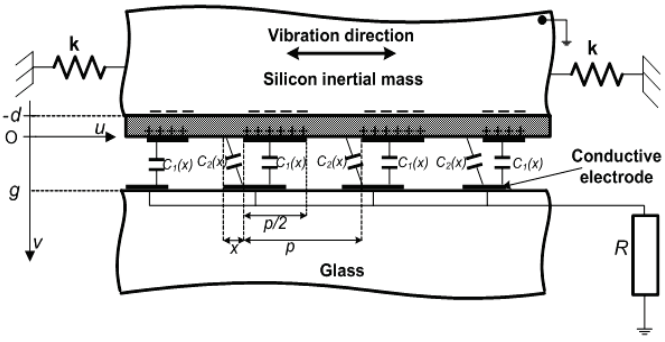

Fig.1: The basic structure of the vibration scavenger. The capacitance values does not depend on d when d<<p.

Capacitance calculation

The plate overlap model for capacitance variation is simple and it can give very useful results in many , situations. In our study, where the emphasis is the reduction of capacitance variation when the gap is not much smaller than the finger electrode width, this model will not work. We have instead considered a situation where the gap size can be much smaller than

the period p, leading to significant fringing field effects. In order to calculate the capacitance variation, the variable capacitance $C_1(x)$ and $C_2(x)$ must be evaluated as functions of the relative mass displacement x, to the fixed electrode. Furthermore, the variation of $C_2(x)$ is identical to that of $C_1(x)$ but shifted by an offset of $p/2$. The capacitance evaluation $C_1(x)$ under fringing field effects is analogous to our own previous work [6]. The calculation is originated from charge distribution on each zero-thickness metal strip m^{th} of the upper electrode (superscript U) and the lower electrode (superscript L). The charge density is formulated by Chebyshev polynomials $T_n(x)$ multiplied by a reciprocal square root form to capture both edge singularities. The formula is based on corresponding expansion coefficients $\{C_n^{U/L}\}$, written by

$$\sigma^{U/L}(u)=\sum_{mn} C_n^{U/L}\frac{T_n\left(\frac{4(u-mp-x^{U/L})}{p}\right)}{\sqrt{1-\frac{16(u-mp-x^{U/L})^2}{p^2}}}\theta\left(\frac{p^2}{16}-(u-mp-x^{U/L})^2\right) \quad (1)$$

where,

$$\theta(x)=\begin{cases}1 & x\geq 0\\ 0 & x<0\end{cases} \quad \text{and} \quad \begin{cases}x^U=x & \text{for the upper electrode}\\ x^L=0 & \text{for the lower electrode}\end{cases}$$

The capacitance value is based on determination of the expansion coefficients $\{C_n^{U/L}\}$. The charge density and the constant potentials $\varphi^{U/L}$ on the upper/lower electrodes can be alternatively expressed by Fourier series with fundamental wave number $k=2\pi/p$. The expansion coefficients are then calculated using Galerkin method with a weight function in the reciprocal square root form. This method is accomplished by enforcing the potentials onto the Chebyshev polynomials to establish the corresponding constant potentials $\varphi^{U/L}$. The expansion coefficients are found by a system of equations represented in form of submatrices $\mathbf{G^{UU}}$, $\mathbf{G^{UL}}$, $\mathbf{G^{LU}}$ and $\mathbf{G^{LL}}$ found in [6], giving

$$\begin{bmatrix}\mathbf{G^{UU}} & \mathbf{G^{UL}}\\ \mathbf{G^{LU}} & \mathbf{G^{LL}}\end{bmatrix}\begin{bmatrix}C_0^U\\ \mathbf{C_1^U}\\ C_0^L\\ \mathbf{C_1^L}\end{bmatrix}=\frac{8\varepsilon_0}{p}\begin{bmatrix}\varphi^U-\varphi_0^{II}\\ \mathbf{0}\\ \varphi^L-\varphi_0^I\\ \mathbf{0}\end{bmatrix} \quad (2)$$

where,

$$\varphi_0^{II}-\varphi_0^I=\frac{\pi g}{4\varepsilon_0}C_0^U=-\frac{\pi g}{4\varepsilon_0}C_0^L$$

As a result, the capacitance $C_1(x)$ is calculated by a relation between the upper and lower charges and the upper and lower potentials. The formula is expressed by

$$C_1(x)=\frac{\varepsilon_0 w}{\frac{g}{p}+\frac{1}{2\pi}(G^{UU}(x)-G^{UL}(x)-G^{LU}(x)+G^{LL}(x))} \quad (3)$$

where the functions $G^{UU}(x)$, $G^{UL}(x)$, $G^{LU}(x)$ and $G^{LL}(x)$ are obtained from elimination of the vectors $\mathbf{C_1^U}$ and $\mathbf{C_1^L}$ in the equation (2).

Fig. 2 illustrates the capacitance variation normalized by the value of a reference capacitance $C_{ref}=\varepsilon_0\frac{pw}{g}$ over one period. At the position of completely overlapping electrodes, the capacitance value with fringing fields is about 0.5 for all values of the ratio p/g. This implies that the fringing field effects are small in this case. Nevertheless, the fringing field effects become considerable when we increase the relative electrode position. At the position of completely non-overlapping electrodes, the normalized capacitance is zero for the parallel plate model, but about 0.39 for our calculations with the ratio p/g=7.

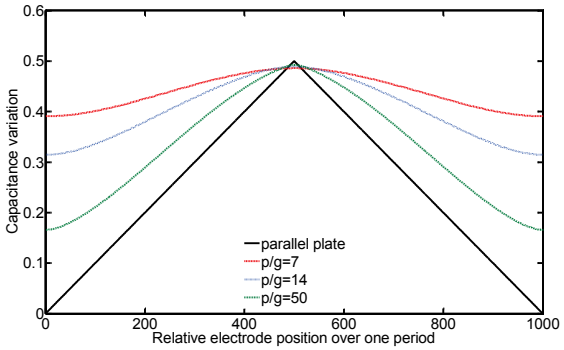

Fig. 2: The variation of $C_1(x)$ for a range of p in x. The variation in $C_2(x)$ would be identical only shifted by $p/2$.

Power calculation

In this work we study the effect of the period of the electrode patterns, and a complex device model is not needed. We accurately model the electrostatic source and its capacitive coupling to an Ohmic load. The mechanical domain is simply described by a sinusoidal vibration of the mass at a frequency ω_m with amplitude x_0. The justification of this approach will be dealt with later in the paper.

The open circuit output voltage of the source can be expressed as:

$$v_g(t)=v_g(x(t))=V_b\frac{C_1(x(t))}{C_1(x(t))+C_2(x(t))} \quad (4)$$

Here V_b is the bias voltage on the charged electrodes and the capacitances are those shown in Fig. 2. It is clear that the waveform $v_g(t)$ will change when x_0 or electrode period changes. This is illustrated in Fig. 3. The upper plots show $v_g(t)$ for one period of mechanical motion with x_0 =300 µm, for two different p values, 70 µm and 500 µm. The plot starts from a maximum overlap position. While the dominant electrical output is at $2\omega_m$, when p=500 µm, it is at $8\omega_m$ when p=70µm. A similar change of output frequency will also result if x_0 increases while p is kept

constant. The curves clearly show an important feature; a decreasing *p/g* leads to an increasing output frequency and a decreasing output voltage.

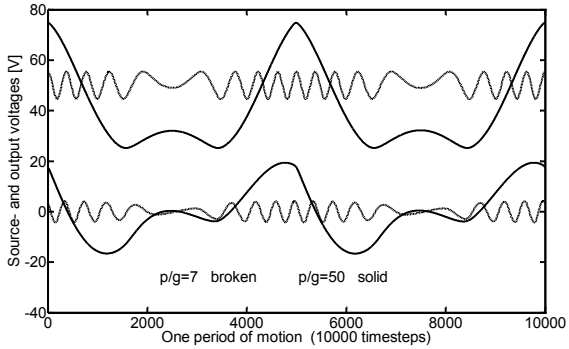

Fig. 3: Generated waveforms before and after RC filtering for two different p/g values.

To optimize the p value at a given value of g and x_0, we must account for the RC coupling made up by the output capacitance, $C_1(x)+C_2(x)$ and the load, R. It is obvious from an electrostatic point of view, and also confirmed by the plots in Fig. 2, that the sum $C_1(x)+C_2(x)$ is constant and independent of x. We are then left with a simple high pass filter model shown in Fig. 4, to maximize the power dissipated in the load resistor. Both the source signal and the second order IIR filter representing the RC network are implemented in MATLAB.

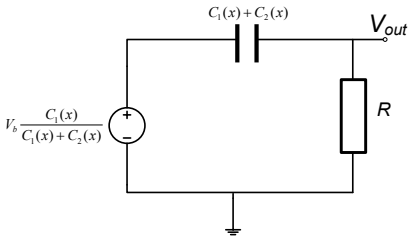

Fig.4: Electrical model of source and load.

The RC coupling creates a high pass filter with $\omega_0=1/RC$. To get a maximum power in R, ω_0 must be in the frequency range of the generated voltage. This implies that the matched load will decrease when the frequency increases as seen in Fig. 3. The matched loads for the two different frequency contents shown,

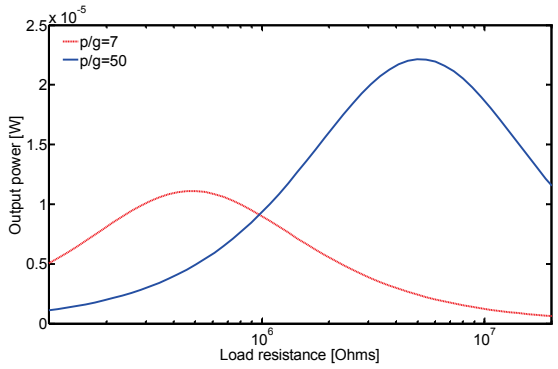

Fig. 5: Output power as function of the load resistance at two values of p/g.

are 5 MΩ for the low frequency and 0.5 MΩ for the high frequency plot. This is more clearly shown in Fig. 5. where the dissipated power is plotted as a function of R for two widely different values of *p/g*, 7 and 50. The plots in Fig. 5 and Fig. 3 refer to the same set of parameters. The low source voltage at $p/g = 7$ is only partly compensated by the lower matched load. An optimal *p/g* giving a max output power may be somewhere between two cases shown.

Optimization

With the modeling tools described we are now in position to study how the electrode period should be chosen when other design parameters are known. To simplify the presentation of the results, we will simply determine the maximum output power, shown as the peak in Fig. 5, as a function of *p/g*. We will in addition include the vibration amplitude, x_0, as a variable. The need for including x_0, is seen from Fig. 3. The two waveforms shown here, both result from x_0=300 µm. A different vibration amplitude will generate waveforms with another frequency content. Since it is the output frequency that determine the matched load, and thereby the output power, we must also study the effect of the vibration amplitude. Fig 6 shows the results. The output power to a matched load is displayed as function of *p/g* in the range between 7 and 100, and x_0 between 0 and 1000 µm. The gap is 10 µm, the electrode transverse width is 5 mm, the length of the electrode pattern is 7 mm and the bias voltage is 100V.

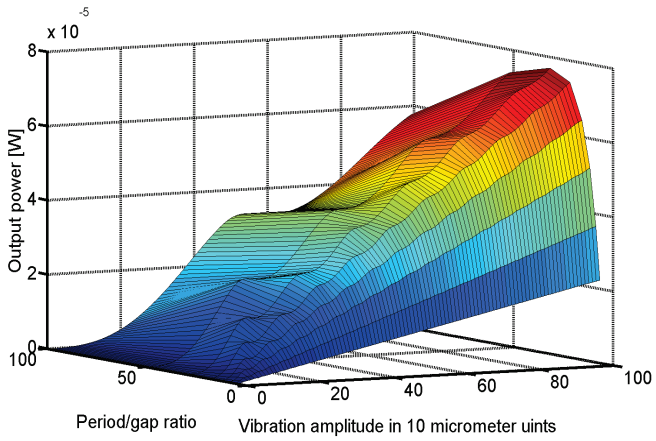

Fig. 6: The output power from a shuttle harvester as function of p/g and x_0.

The calculated output level is in the tens of µW range. It is the result of simulation with parameters that may well exist in a real device, but in the present context we should focus on the variation as function the variables and not on the power level itself.

DISCUSSION

The model

In our model the fringing field effects in the electrodes are treated with high accuracy. We must do so, since these effects leads to the reduction of capacitance variation when the *p/g* ratio is made smaller. If we instead use a plate overlap model, the capacitance variation and thereby the generated voltage, will stay constant. This will not lead to an optimal value of p/g, balancing the amplitude and the frequency of the generated waveform.

The model uses, on the other hand, a very simple account of the dynamics and the electrostatic forces between the electrodes. This may be done since the end result with a more refined model, at least with narrow band vibration, is a motion with amplitude x_0 and frequency ω_m that are only weakly affected by changes in the p/g-ratio

Simulation results

When we return to the result of our simulations in Fig. 6, we see the expected result of changes in *p/g*. For all values of x_0, the output power rises with an increasing *p/g*, reaches a maximum and then decreases. There are some peaks and walleyes in the plotted surface, which we must also consider. They are most clearly seen at *p/g*=100 where a peak appears at x_0=500 µm. A similar peak is seen at x_0=250 µm for *p/g*=50. In general peaks are located at $x_0=n \cdot p/2$. The reason for this can be understood from the waveform in Fig 3. When x_0 coincides with a number of half periods of the electrode pattern, the generated voltages will be a complete number of periods with full peak to peak range between the max and the min value. In the figure this requirement is not met, $x_0=1.2 \cdot p/2$ for the solid curve. Two electrical periods have high amplitude and two periods have low. If $x_0=2 \cdot p/2$ or 500 µm, the waveform will have 4 periods of high amplitude. This corresponds to one of the peaks of the surface in Fig. 6. We also see that the size of the peaks increase when *p/g* increases. On the other hand, we approach a linear relation between x_0 and power output when x_0/p becomes large.

The features discussed above have less influence on the relation between max power and *p/g* at higher values of x_0. Above x_0=500 µm the highest output appears at *p/g*=30. The peak is quite broad and the variation between *p/g*=20 and 40 is typically +/- 5 %. This agrees well with [4], where the optimum was found at *p/g*=22.

CONCLUSION

We have simulated the power generation in an electrostatic shuttle harvester. The aim has been to determine the period of the electrode pattern that gives us the highest generated output power. When the gap size is given, we find the highest output when the period equals $30 \cdot g$.

For a linear relation between power and x_0 the period should also be much less than $x_0/2$, half the mechanical amplitude. If x_0 is small this leads to a narrow gap. This is positive, since it results in a low source impedance, but from a fabrication point of view it may be challenging.

ACKNOWLEDGEMENT

This work was in part supported by the Research Council of Norway through grant 191282.

REFERENCES

[1] Naruse Y, Matsubara N, Mabuchi K, Izumi M, Honma K 2008 Electrostatic micro power generator from low frequency vibration such as human motion *Technical Digest PowerMEMS 2008 (Sendai, Japan, 9-12 November 2008)* 19-22

[2] Miki D, Honzumi M, Suzuki Y, Kasagi N 2009 MEMS electret generator with electrostatic levitation *Technical Digest PowerMEMS 2009 (Washington DC, USA, 1-4 December 2009)* 169-173

[3] Husa S 2007 An analytic treatment of the transduction in a shuttle type vibration energy harvester *Technical Digest PowerMEMS 2007 (Freiburg, Germany, 28-29 November 2007)* 113-116

[4] Boisseau S, Despesse G, Sylvestre A 2010 Optimization of an electret-based energy harvester Smart Mater. Struct. **19** 7 075015 (10pp).

[5] Halvorsen E, Westby E R, Husa S, Vogl A, Østbø N P, Leonov V, Sterken T, Kvisterøy T 2009 An electrostatic energy harvester with electret bias *Technical Digest Transducers 2009 (Denver, Colorado, USA, 21-25 June 2009)* 1381-1384.

[6] Le C P, Halvorsen E 2009 Evaluation of parameters for electrostatic harvesters *Technical Digest DTIP 2009 (Rome, Italy, 1-3 April 2009)* 286-291